A&A 484, 327–340 (2008)
DOI: 10.1051/0004-6361:200809622

Astronomy & Astrophysics

GMRT radio halo survey in galaxy clusters at z = 0.2–0.4

II. The eBCS clusters and analysis of the complete sample

T. Venturi[1], S. Giacintucci[1,2], D. Dallacasa[3,1], R. Cassano[3,1], G. Brunetti[1], S. Bardelli[4], and G. Setti[3,1]

[1] INAF – Istituto di Radioastronomia, via Gobetti 101, 40129 Bologna, Italy
e-mail: tventuri@ira.inaf.it
[2] Harvard-Smithsonian Center for Astrophysics, 60 Garden Street, Cambridge, MA02138, USA
[3] Dipartimento di Astronomia, Università di Bologna, via Ranzani 1, 40126 Bologna, Italy
[4] INAF – Osservatorio Astronomico di Bologna, via Ranzani 1, 40127 Bologna, Italy

Received 20 February 2008 / Accepted 19 March 2008

ABSTRACT

Aims. We present the results of the GMRT cluster radio halo survey. The main purposes of our observational project are to measure what fraction of massive galaxy clusters in the redshift range z = 0.2–0.4 host a radio halo, and to constrain the expectations of the particle re-acceleration model for the origin of the non-thermal radio emission.
Methods. We selected a complete sample of 50 clusters in the X-ray band from the REFLEX (27) and the eBCS (23) catalogues. We present Giant Metrewave Radio Telescope (GMRT) observations at 610 MHz for all clusters still lacking high sensitivity radio information, i.e. 16 eBCS and 7 REFLEX clusters, thus completing the radio information for the whole sample. The typical sensitivity in our images is in the range $1\sigma \sim 35$–100 μJy b^{-1}.
Results. We found a radio halo in A 697, a diffuse peripheral source of unclear nature in A 781, a core-halo source in Z 7160, a candidate radio halo in A 1682 and "suspect" central emission in Z 2661. Including the literature information, a total of 10 clusters in the sample host a radio halo. A very important result of our work is that 25 out of the 34 clusters observed with the GMRT do not host extended central emission at the sensitivity level of our observations, and for 20 of them firm upper limits to the radio power of a giant radio halo were derived. The GMRT Radio Halo Survey shows that radio halos are not common, and our findings on the fraction of giant radio halos in massive clusters are consistent with the statistical expectations based on the re-acceleration model. Our results favour primary to secondary electron models.

Key words. radio continuum: galaxies – galaxies: clusters: general

1. Introduction and the GMRT radio halo survey

Radio and X-ray observations of galaxy clusters prove that the intracluster medium (ICM) in clusters of galaxies is a mixture of hot plasma, magnetic field and relativistic particles. While X-ray observations reveal the presence of diffuse hot gas, the spectacular synchrotron radio emission extended on the Mpc scale and observed in a growing number of massive clusters is the signature of the the presence of relativistic electrons (with Lorentz factor $\gamma \gg 1000$) and magnetic fields spread over the whole cluster volume (e.g. Feretti 2005). Recent studies revealed that the magnetic fields in galaxy clusters are weak, with strengths in the range ~0.1–1 μG (for recent reviews see Govoni & Feretti 2004; Ferrari et al. 2008). The recently discovered hard X-ray tails in excess of the thermal Bremsstrahlung spectrum in a few galaxy clusters (Fusco-Femiano et al. 2004; Rephaeli et al. 2008; Fusco-Femiano & Orlandini 2008) are also considered evidence in favour of a non-thermal component in the ICM (see also Rossetti & Molendi 2007, for further discussion on this issue).

The extended cluster radio emission may take the form of *radio halos*, *relics* and *core-halos* (or mini-halos). While the latter reach extensions of the order of $\lesssim$500 kpc, are associated with the dominant galaxy in cooling core clusters and are thought to be related to the radio emission of the central AGN, halos and relics are much larger in size (reaching and exceeding the Mpc scale) and are not associated with AGN activity in individual galaxies. *Radio halos* are usually located at the centre of galaxy clusters, and show a fairly regular morphology; *relics* are found at the cluster periphery, are highly polarized and exhibit a variety of radio morphologies, the most common being sheet, arc or toroid. There is some consensus on the fact that the origin of radio relics resides in cluster mergers and/or matter accretion: the strong peripheral shocks developing during these energetic events may be efficient particle accelerators (Sarazin 1999; Ryu 2003; Pfrommer 2006).

The origin of the synchrotron radio emission in halos is still an open problem, since the life-time of the electrons emitting synchrotron radiation is much shorter than the diffusion time necessary to cover their large extent, typically of the order of a Mpc.

Historically, two main possibilities have been suggested to account for the existence of radio halos: (1) "re-acceleration models", or "primary electron" models, where electrons are re-accelerated in-situ, due to the turbulence injected in the cluster volume by massive merger events (e.g. Brunetti et al. 2001; Petrosian 2001; and the review papers by Brunetti 2003; Sarazin 2004; Petrosian & Bykov 2008); (2) "secondary electron models", which predict that relativistic electrons are secondary products of hadronic collisions between the ICM and cosmic rays (e.g. Dennison 1980; Blasi & Colafrancesco 1999; Dolag & Enßlin 2000).

The re-acceleration scenario implies a tight connection between the process of hierarchical cluster formation and the non-thermal phenomena, and indeed there is observational evidence that radio halos are found in clusters with signatures of ongoing merging processes (e.g. Buote 2001; Schuecker et al. 2001), and that the occurrence of radio halos increases with the X-ray luminosity of the parent clusters (Giovannini et al. 1999; Cassano et al. 2008).

Growing attention has been given to the statistical properties of radio halos in the framework of this model. Calculations were developed in order to model the connection between radio halos and the merging history of galaxy clusters. Expectations were made for the occurrence of *giant*[1] radio halos as a function of redshift and mass (Cassano & Brunetti 2005, hereinafter CB05; Cassano et al. 2006, hereinafter CBS06; Cassano et al. 2008). The predictions show that the bulk of giant radio halos is expected in the redshift range $z = 0.2$–0.4, where a fraction of $\sim$35% of massive clusters ($M > 10^{15}\ M_{\odot}$) may host such cluster radio sources.

In order to investigate the connection between cluster mergers and the presence of diffuse sources in galaxy clusters, and to test the statistical predictions, we selected a complete sample of 50 massive galaxy clusters in the redshift range $z = 0.2$–0.4, and carried out a deep pointed radio survey with the Giant Metrewave Radio Telescope (GMRT, Pune, India) at 610 MHz, imaging all clusters in the sample lacking high sensitivity information. We refer to this project as the "GMRT radio halo survey". In Venturi et al. (2007, hereinafter Paper I) we reported the results on 11 observed clusters.

In this paper we present the completion of the GMRT radio halo survey. The paper is organised as follows: in Sect. 2 we present the sample; in Sect. 3 we describe the radio observations; in Sects. 4 and 5 we present the results; in Sect. 6 we discuss the results of the GMRT radio halo survey as a whole; the summary and conclusions in the light of the re-acceleration model are given in Sect. 7.

The cosmology adopted in this paper is $H_0 = 70$ km s^{-1} Mpc^{-1}, $\Omega_{\rm m} = 0.3$ and $\Omega_{\Lambda} = 0.7$. We assume $S \propto \nu^{-\alpha}$ throughout the paper.

2. The cluster sample

From the ROSAT–ESO Flux Limited X-ray galaxy cluster catalogue (REFLEX, Böhringer et al. 2004) and from the extended ROSAT Brightest Cluster Sample catalogue (BCS, Ebeling et al. 1998, 2000) we selected all clusters satisfying the following constraints:

1) $L_{\rm X}(0.1$–$2.4\ {\rm keV}) > 5 \times 10^{44}\ {\rm erg\,s^{-1}}$;
2) $0.2 < z \leq 0.4$;
3) $-30^{\circ} < \delta < +2.5^{\circ}$ for the REFLEX sample; $15^{\circ} < \delta < 60^{\circ}$ for the eBCS sample.

The limit in X-ray luminosity comes from the need to select massive clusters, which are expected to host a giant radio halo (Cassano, et al. 2004, and CB05). The limit in $L_{\rm X}$ corresponds to a limit in virial mass $M_{\rm V} > 1.4 \times 10^{15}\ M_{\odot}$, assuming the relation $L_{\rm X}$–$M_{\rm V}$ derived in CBS06 (see also Paper I).

The value $\delta = 2.5^{\circ}$ is the REFLEX declination limit; the lower limit $\delta > -30^{\circ}$ was chosen to ensure good u-v coverage with the GMRT. In order to reach a compromise between the need to obtain a large sample and the observational effort necessary to complete the requested radio information, we selected from the eBCS catalogue all clusters in the declination range $15^{\circ} < \delta < 60^{\circ}$. The final full sample includes 50 clusters, 27 from the REFLEX catalogue and 23 from the eBCS. The complete list of clusters is reported in Table 1, where we provide the following information: (1) cluster name (either from optical or from X-ray catalogues); (2) $\rm RA_{J2000}$ and (3) $\rm Dec_{J2000}$; (4) redshift; (5) X-ray luminosity; (6) notes on the radio information. The upper part of the Table refers to the REFLEX clusters (see also Paper I), the lower part to the eBCS catalogue. Note that the cluster RXCJ 2228.6+2037 has $z = 0.4177$, i.e. just above our selection limit. We included it in the sample observed at the GMRT, but it has not been considered in our discussion (Sect. 6) and in the statistical analysis carried out in Cassano et al. (2008).

3. Radio observations and data reduction

We carried out GMRT observations at 610 MHz for the 23 clusters listed in Table 1 still lacking proper imaging at low resolution to assess the presence of extended radio emission on the cluster scale, i.e. 7 REFLEX and 16 eBCS clusters (see last column in the table). The observations were performed during three observing runs. Most of the clusters (21) were observed during the period between 30 September 2005 and 04 October 2005; A 2645 and A 2667 were observed on 27 August 2006; A 1682 was observed during the 2005 run, but it was reobserved on 05 December 2006, due to the poor quality of the first dataset, which did not allow proper imaging.

Each cluster was observed for a total of 2.5–3 h, with a duty cycle of 24 min on the target and 6 min on the phase calibrator. Depending on the allocated LST intervals, the observations for each cluster covered a hour angle in the range 3–5 h.

The data were recorded simultaneously using the upper and lower side bands (USB and LSB respectively), for a total bandwidth of 32 MHz. The default spectral line observing was performed, with each individual band divided into 128 channels, with a spectral resolution of 125 kHz/channel.

The data analysis was carried out using the standard tasks of the NRAO AIPS (Astronomical Image Processing System) package. After bandpass calibration and removal of the channels at the edges of the band, the remaining 94 channels were averaged into 6 channels. The USB and LSB datasets were calibrated and self-calibrated independently, and the final images were obtained on the image plane by combining the final images from each individual dataset. Multifield imaging was carried out in each step of the data reduction, to account for the non-coplanarity of the sky within the large field of view of the primary beam at 610 MHz.

The full resolution of the GMRT at 610 MHz is $\sim 5''$ and the largest nominal detectable structure is $17'$. This scale is much larger than the typical angular scale of Mpc-size radio halos in the redshift interval under consideration here, which ranges from $\sim 3'$ at $z = 0.4$ to $\sim 5'$ at $z = 0.2$. This ensures the detection of the Mpc size radio sources we are investigating (see Sect. 4 for a detailed discussion on this point).

Beyond the full resolution images, produced with uniform weighting and no tapering, for each field we produced images with different resolutions, tapering the u-v data by means of the parameters `robust` and `uvtaper` in the task IMAGR. A typical "low" resolution is of the order of $20''$–$25''$.

The rms noise (1σ level) in the final images ranges from $\sim 40\ \mu$Jy b^{-1} in the best cases, to 100–140 μJy b^{-1} in the worst. Most of the fields have an rms of the order of 50–80 μJy b^{-1}.

[1] Linear size $\gtrsim$1 Mpc as defined in CB05, with $H_0 = 50$ km s^{-1} Mpc^{-1}. This size corresponds to $\gtrsim$ 700 kpc with the cosmology assumed in this paper.

Table 1. Cluster sample from the REFLEX and eBCS catalogues.

Cluster name	RA_{J2000}	Dec_{J2000}	z	L_X(0.1–2.4 keV) 10^{44} erg s^{-1}	Notes
REFLEX Sample					
A 2697	00 03 11.8	–06 05 10	0.2320	6.88	Paper I
A 2744	00 14 18.8	–30 23 00	0.3066	12.92	(1)
A 2813	00 43 24.4	–20 37 17	0.2924	7.62	This paper
A 141	01 05 34.8	–24 39 17	0.2300	5.76	Paper I
A 2895	01 18 11.1	–26 58 23	0.2275	5.56	This paper
A 209	01 31 53.0	–13 36 34	0.2060	6.29	Paper I
A 3088	03 07 04.1	–28 40 14	0.2537	6.95	Paper I
RXCJ 0437.1+0043	04 37 10.1	+00 43 38	0.2842	8.99	(2)
A 521	04 54 09.1	–10 14 19	0.2475	8.18	Paper I, (3)
RXCJ 0510.7–0801	05 10 44.7	–08 01 06	0.2195	8.55	√
A 3444	10 23 50.8	–27 15 31	0.2542	13.76	Paper I
RXCJ 1115.8+0129	11 15 54.0	+01 29 44	0.3499	13.58	This paper
A 1300	11 31 56.3	–19 55 37	0.3075	13.97	(4)
RXCJ 1212.3–1816	12 12 18.9	–18 16 43	0.2690	6.20	√
RXCJ 1314.4–2515	13 14 28.0	–25 15 41	0.2439	10.94	Paper I, (2)
S 780	14 59 29.3	–18 11 13	0.2357	15.53	Paper I
RXCJ 1504.1–0248	15 04 07.7	–02 48 18	0.2153	28.08	√
RXCJ 1512.2–2254	15 12 12.6	–22 54 59	0.3152	10.19	This paper
RXCJ 1514.9–1523	15 14 58.0	–15 23 10	0.2226	7.16	√
A 2163	16 15 46.9	–06 08 45	0.2030	23.17	(5), (6)
RXCJ 2003.5–2323	20 03 30.4	–23 23 05	0.3171	9.25	Paper I
RXCJ 2211.7–0350	22 11 43.4	–03 50 07	0.2700	7.42	√
A 2485	22 48 32.9	–16 06 23	0.2472	5.10	This paper
A 2537	23 08 23.2	–02 11 31	0.2966	10.17	Paper I
A 2631	23 37 40.6	+00 16 36	0.2779	7.57	Paper I
A 2645	23 41 16.8	–09 01 39	0.2510	5.79	This paper
A 2667	23 51 40.7	–26 05 01	0.2264	13.65	This paper
eBCS Sample					
RXJ 0027.6+2616	00 27 49.8	+26 16 26	0.3649	12.29	This paper
A 611	08 00 58.1	+36 04 41	0.2880	8.86	This paper
A 697	08 42 53.3	+36 20 12	0.2820	10.57	This paper
Z 2089	09 00 45.9	+20 55 13	0.2347	6.79	This paper
A 773	09 17 59.4	+51 42 23	0.2170	8.10	(1)
A 781	09 20 23.2	+30 26 15	0.2984	11.29	This paper
Z 2661	09 49 57.0	+17 08 58	0.3825	17.79	This paper
Z 2701	09 52 55.3	+51 52 52	0.2140	6.59	This paper
A 963	10 17 09.6	+39 01 00	0.2060	6.39	This paper
A 1423	11 57 22.5	+33 39 18	0.2130	6.19	This paper
Z 5699	13 06 00.4	+26 30 58	0.3063	8.96	This paper
A 1682	13 06 49.7	+46 32 59	0.2260	7.02	This paper
Z 5768	13 11 31.5	+22 00 05	0.2660	7.47	This paper
A 1758a	13 32 32.1	+50 30 37	0.2800	12.26	(7)
A 1763	13 35 17.2	+40 59 58	0.2279	9.32	VLA Archive
Z 7160	14 57 15.2	+22 20 30	0.2578	8.41	This paper
Z 7215	15 01 23.2	+42 21 06	0.2897	7.34	This paper
RXJ 1532.9+3021	15 32 54.2	+30 21 11	0.3450	16.49	This paper
A 2111	15 39 38.3	+34 24 21	0.2290	6.83	VLA Archive
A 2219	16 40 21.1	+46 41 16	0.2281	12.73	(8)
A 2261	17 22 28.3	+32 09 13	0.2240	11.31	VLA Archive
A 2390	21 53 34.6	+17 40 11	0.2329	13.43	(8)
RXJ 2228.6+2037	22 28 34.4	+20 36 47	0.4177	19.44	This paper

References: Paper I: Venturi et al. (2007); (1) Govoni et al. (2001); (2) Feretti et al. (2005); (3) Giacintucci et al. (2006); (4) A 1300 Reid et al. (1999); (5) Herbig & Birkinshaw (1994); (6) Feretti et al. (2001); (7) Giovannini et al. (2006); (8) Bacchi et al. (2003); √ clusters which are part of the GMRT cluster Key Project (P. I. Kulkarni).

For each cluster the rms in the full resolution and tapered images are comparable. The quality of the final images depends on the usable bandwidth (in a number of cases only one of the two bands provided good data) and on the presence of strong sources in the proximity of the field centre. We estimate that the residual amplitude calibration uncertainty is of the order of $\lesssim$5%.

In Table 2 we list the convolution beam of the final images produced at the lowest resolution (Col. 2) and referred to in this paper (Sect. 4), the average rms, estimated over regions far from strong sources (Col. 3); a note concerning the detection of cluster scale radio emission (Col. 4).

Table 2. GMRT observations.

Cluster	Beam, PA arcsec, °	rms μJy b^{-1}	Notes°
RXJ 0027.6+2616	15.4 × 11.2, 53.6	65	
A 2813	13.9 × 11.6, 29.6	130	
A 2895⋆	9.0 × 5.1, 36.3	140	
A 611	13.5 × 12.0, 60.0	50	
A 697	40.0 × 35.0, 37.0	50	GRH
Z 2089	15.4 × 13.7, 14.0	45	
A 781	18.0 × 15.0, 0.0	50	DE
Z 2701	24.5 × 16.3, 43.0	75	
Z 2661	20.0 × 20.0, 0.0	65	C
RXCJ 1115.8+0129	17.0 × 10.0, 0.0	45	
A 963⋆	6.0 × 4.5, 65.0	150	
A 1423	22.5 × 14.0, 45.5	85	
Z 5699	20.0 × 13.6, 57.2	75	
A 1682	20.3 × 13.9, 86.0	80	C
Z 5768	20.6 × 16.8, 39.1	70	
Z 7160	17.0 × 14.0, 0.0	40	c–H
Z 7215	23.0 × 18.0, −0.9	100	
RXCJ 1512.2−2254	19.6 × 16.9, 23.6	80	
RXJ 1532.9+3021	24.0 × 21.0, 19.9	80	
RXJ 2228.6+2037	22.5 × 18.0, −5.8	80	
A 2485	16.1 × 12.7, 35.3	130	
A 2645⋆	10.8 × 6.4, 32.5	250	
A 2667	17.0 × 13.7, 33.1	100	

⋆ Due to the presence of strong confusing sources, low resolution images could not be produced. ° Notes on the radio emission: GRH = giant radio halo; DE = diffuse emission at the cluster periphery; C = candidate emission at the cluster centre (positive residuals); c–H = core-halo.

4. Non-detections and upper limits

Most of the clusters observed with the GMRT radio halo survey do not show any hint of radio emission on the cluster scale at the sensitivity of the observations, as is clear from Table 2 and Paper I. In order to provide quantitative observational information it is crucial to place firm upper limits on the radio power for the non detection of radio halos in our sample. From an observational point of view this means to place upper limits on the flux density from the final images.

4.1. The procedure

We approached the problem following the steps described below.

1) We modelled the brightness profiles of well studied radio halos with sets of optically thin concentric spheres with different radius and flux density, and obtained "families" of radio halos with steps in total flux density and angular scale (see also Brunetti et al. 2007, hereinafter BVD07, and Fig. 1 therein). In particular,in each model the largest sphere contains ∼50% of the total flux.
2) Each model of the the brightness distribution, which we will refer to as the "fake" radio halo, was injected in a number of selected u–v datasets with the task UVMOD in AIPS. This task transforms the brightness distribution of the model into u–v components, adds them to the original data and produces a new "modified" u–v dataset.
3) Imaging was carried out on each of the "modified" u–v datasets by means of the task IMAGR in AIPS. From the "modified" datasets we subtracted the individual sources in the central area of the cluster and imaged the residual emission.
4) We finally integrated the flux density (task TVSTAT) over an area as large as the angular scale of the injected radio halo.

From the datasets presented here, we chose representative clusters for our analysis exploring the rms range of our observations (see Table 2), whose final images do not show hints of extended emission in the cluster central area. As a further test of our procedure we injected the "fake" radio halos both at the cluster centre and in a nearby empty region (free from point sources and artifacts). The largest angular scale (LAS) of the "fake" radio halos explores the range from 180″ to 320″, so as to cover the angular scale corresponding to a linear size of 1 Mpc in the redshift interval 0.2–0.4, (see Sect. 3). We injected total flux density values $S_{\rm inj}$ from 3 to 30 mJy and produced images at different resolutions, in the range 10″–25″.

4.2. The results

We found that the component of the "fake" radio halos with the largest angular size (i.e. the one with lowest brightness) is at least partly lost in the imaging process, the effect becoming more important for faint flux densities and/or large angular sizes. On the other hand, the central regions, i.e. those with higher surface brightness, are usually well imaged. Thus, about up to ∼50% of the injected flux density is lost. As a consequence of this result, the LAS in the imaged fake halos is usually smaller than the one injected. For clear detections, the measured LAS is of the order of ∼70% of the injected one.

A conservative conclusion of our procedure is that above a value $S_{\rm inj} \sim 12$ mJy the presence of extended emission may be safely established over all ranges of angular scales considered in our analysis. Injected flux densities of the order of 7–10 mJy result in positive residuals with integrated flux density above the noise level (i.e. ∼3–5σ), which would lead to "suspected" emission. Therefore these values may be considered upper limits to the radio halo flux density for those clusters where no evidence of central residual emission is found.

In Fig. 1 we report a sequence of images with constant LAS and varying flux density (upper panels) and constant flux density and varying LAS (middle panel in the upper frame and lower panel). The panels in the figure highlight the dependence of the imaged "fake" halos on $S_{\rm inj}$ and LAS, and also show that the angular scales are smaller than those injected.

This procedure makes use of true GMRT u-v datasets, therefore our conclusions on the detection limit of radio halos apply to the observations presented here and in Paper I.

For each cluster observed with the GMRT (see Table 1) lacking extended emission in our images, we derived the upper limit to the radio power (expressed in W Hz^{-1}) following BVD07. Our results are reported in Table 3, which provides upper limits for 20 clusters. The upper part of the table refers to the REFLEX sample, the lower part to the eBCS. For a consistent analysis, the rms values given for those clusters presented in Paper I refer to low resolution images, and this accounts for some minor differences between the values presented here and those in Table 2 of Paper I.

Table 3 does not include the clusters with rms $\geq 130\,\mu$Jy b^{-1}, i.e. A 2813, A 2895, A 2845, A 2645, A 963 (see Table 2). For all of them only part of the visibilities could be used in the imaging process, due to a number of different problems occurring during the observations, and any limit set for them would not be significant. These five clusters were not included in the analysis carried out in BVD07.

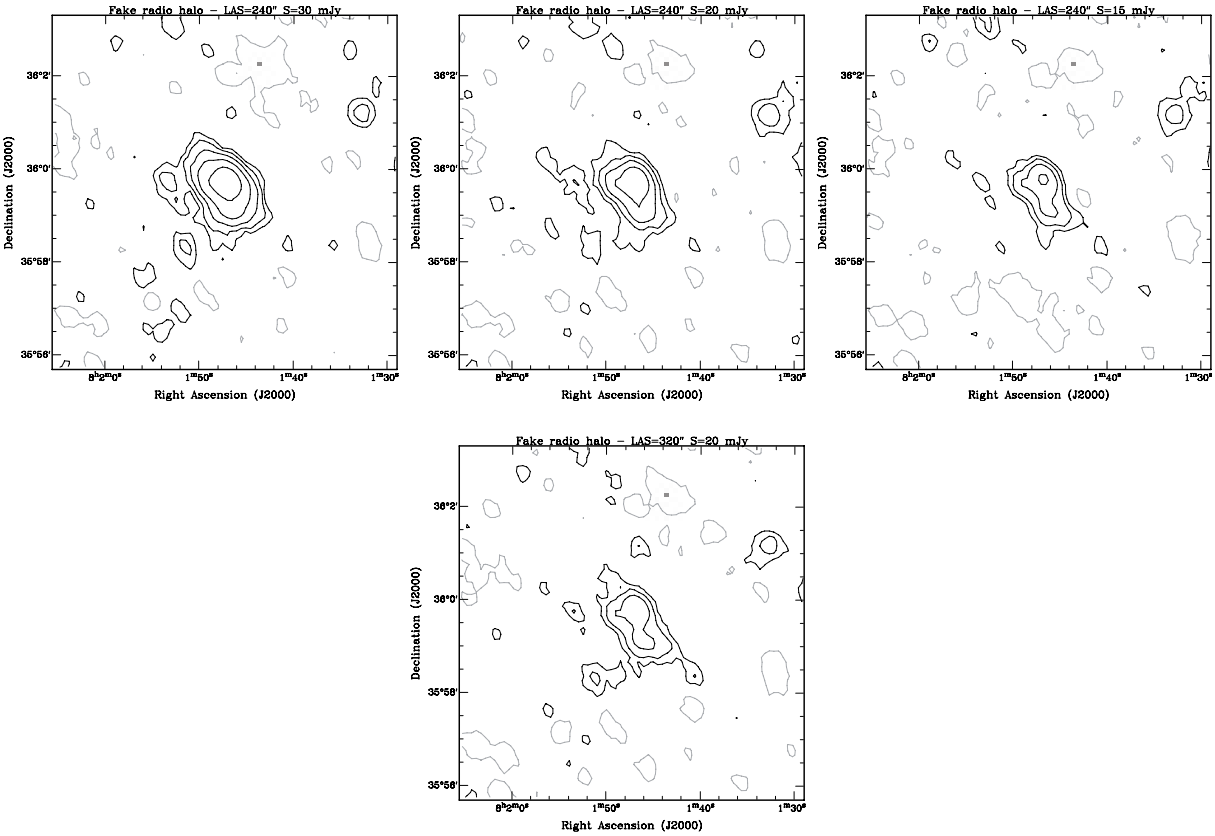

Fig. 1. 610 MHz contours of "fake" radio halos. *Upper frame* – Sequence with fixed LAS = 240″ and decreasing flux density. $S_{\rm inj}$ = 30, 20 and 15 going *from left to right*. The restoring beam is 30″ × 24″; the contour levels start from 0.15 mJy b^{-1} and increase by factor of 2. *Lower frame* – An example with $S_{\rm inj}$ = 20 mJy LAS = 320″, to be compared to the *central panel* in the upper frame. Restoring beam and contour levels as in the upper frame.

Table 3. Radio power upper limits for all undetected radio halos in the GMRT radio halo survey.

Cluster Name	z	rms μJy b^{-1}	Log $P_{610\ \rm MHz}$ W Hz^{-1}
A 2697	0.2320	80	24.05
A 141	0.2300	90	24.07
A 3088	0.2537	65	24.07
RXCJ 1115.8+0129	0.3499	45	24.10⋆
S 780	0.2357	65	24.02
RXCJ 1512.2−2254	0.3152	80	24.20
A 2537	0.2966	65	24.15⋆
A 2631	0.2779	60	24.05
A 2667	0.2264	100	24.09
RXCJ 0027.6+2616	0.3649	65	24.30
A 611	0.2880	50	24.07
A 781	0.2984	50	24.00⋆
Z 2089	0.2347	45	23.86
Z 2701	0.2140	75	23.98⋆
A 1423	0.2130	85	24.02
Z 5699	0.3063	75	24.20
Z 5768	0.2660	70	24.00
Z 7215	0.2897	100	24.20
RXCJ 1532.9+3021	0.3450	80	24.25
RXCJ 2228.6+2037	0.4177	80	24.40⋆

⋆ These upper limits are about ∼20% deeper than those used in BVD07, due to improved images prepared for this paper.

We remind here that a radio halo was found in the clusters A 209, RXCJ 1314.4–2515 and RXCJ 2003.5–2323; extended emission was found around the central galaxy in A 3444 (Paper I); "suspect" extended emission has been found in A 521 at 327 MHz (Giacintucci et al. 2008) and follow-up analysis is in progress (Brunetti et al., in prep.). Hence, these clusters are not included in the analysis. We also excluded from the list A 697, Z 7160, A 1682 and Z 2661 (see Table 2), which will be presented in detail in the next Section.

5. Cluster scale radio emission: new detections and candidates

Table 2 summarizes the results of the observations presented in this paper. Cluster scale radio emission in the form of giant radio halo, core-halo and peripheral emission was detected respectively in A 697, Z 7160 and A 781. Furthermore positive residuals, which may suggest the presence of diffuse sources, were found in A 1682 and Z 2661. In this section we will present and briefly discuss these results.

5.1. The giant radio halo in A 697

No high sensitivity radio imaging is available in the literature for A 697 (z = 0.2820, richness class 1, Bautz-Morgan type II–III). Inspection of the cluster centre in the NRAO VLA Sky Survey (NVSS; Condon et al. 1998) is not very helpful, due to the presence of residual fringes in the image. Kempner & Sarazin (2001) reported the presence of candidate extended emission at the cluster centre on the basis of inspection of the 327 MHz Westerbork Northern Sky Survey image (WENSS; Rengelink et al. 1997).

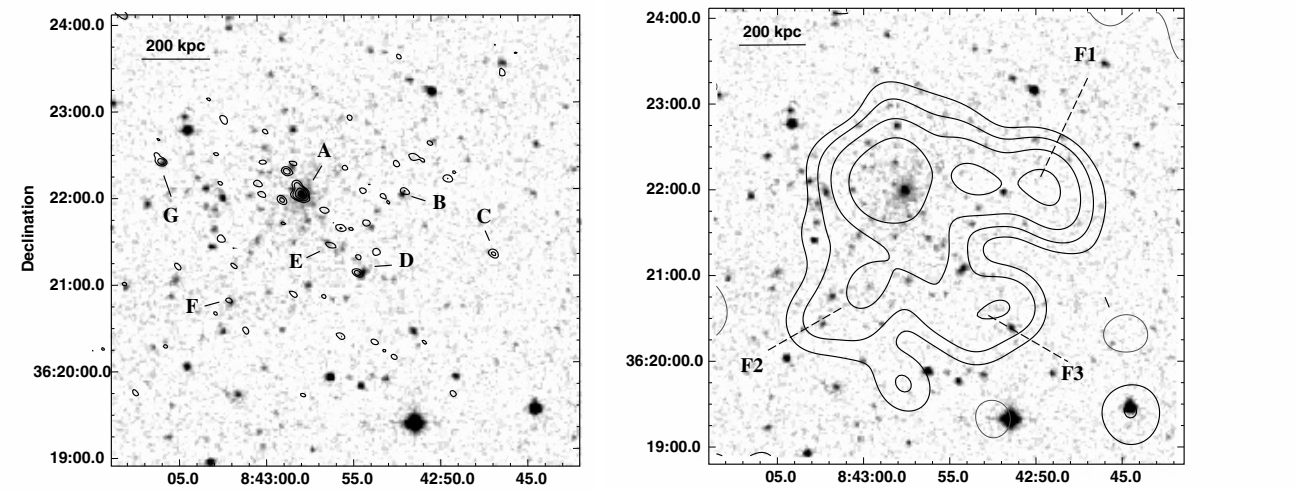

Fig. 2. *Left* – 610 MHz GMRT radio contours of A 697, overlaid on the DSS–2. The resolution of the image is 6″ × 5″. The contour levels are ±0.075, 0.15, 0.3, 0.6, 1.2, 2.4, 4.8, 9.6 mJy b^{-1}. The rms level (1σ) is 25 μJy b^{-1}. *Right* – Same portion of the radio sky with a 610 MHz 40″ × 35″ image overlaid. The radio contours are ±0.15, 0.3, 0.6, 1.2, 2.4, 4.8, 9.6 mJy b^{-1}. The rms level (1σ) is 50 μJy b^{-1}. For this cluster 1″ = 4.232 kpc.

An image of the central part of A 697 at 610 MHz is shown in Fig. 2, overlaid on the red optical frame from the Digitized Palomar Sky Survey (DSS–2). The full resolution image (left panel) shows a number of discrete radio sources which are labelled from A to G. Source A is identified with the central cD galaxy; source B is associated with a backgroud galaxy, as derived from the redshift information in the Sloan Digital Sky Survey (SDSS); all the other sources have an optical counterpart at the redshift of the cluster according to the spectroscopic catalogue in Girardi et al. (2006) and to the SDSS. In addition to the individual radio galaxies, positive residuals of radio emission are clearly visible. After subtraction of the flux density of the radio galaxies, which contribute a total of 2.3 mJy, these residuals account for ∼9 mJy, suggesting the presence of low surface brightness emission at the cluster centre.

In order to highlight such emission, we subtracted from the *u-v* data all the individual sources visible in the full resolution image, and produced an image with a resolution of 40″ × 35″. This image is shown in the right panel of Fig. 2, and confirms the existence of extended emission in the form of a giant radio halo, which extends on a largest angular scale LAS ∼ 3.5′, corresponding to a largest linear size LLS ∼ 890 kpc. Its total flux density, after subtraction of the individual radio galaxies (from A to G in left panel of Fig. 2) is $S_{610\ \mathrm{MHz}}$ = 13 mJy, which implies a total radio power of $P_{610\ \mathrm{MHz}} = 3.5 \times 10^{24}$ W Hz^{-1}. The average surface brightness of the halo is of the order of $\sim 5 \times 10^{-4}$ mJy arcsec^{-2}. This flux density value should be considered a lower limit. Indeed, on the basis of our analysis on the upper limits (Sect. 4) we estimate that a fraction of the flux density of the order of ∼30% (from the outermost low brightness regions) may have been lost for this source.

The overall morphology of the giant radio halo is rather complex. The inner part of the source, i.e. a region of ∼1′ radius around the cluster centre, appears regular and symmetric. At larger radius a bright filament of emission (labelled as F1 in the right panel of Fig. 2) extends in the western direction, and two fainter features (F2 and F3) are located South of the cluster centre. The emission detected in the WENSS image (Kempner & Sarazin 2001) appears elongated westward of the source peak. This elongation may correspond to the filament F1 observed at 610 MHz. The southern emission is undetected in the WENSS image. However, we note that the very low brightness of the radio halo in the outer parts does not allow a detailed comparison of the fainter features.

An optical and X-ray analysis of A 697 was carried out by Girardi et al. (2006), who found that the cluster is experiencing a very complex merging process. They argued that the dynamical state of A 697 might be explained either as an ongoing multiple accretion of small clumps by a very massive cluster, or as the result of a major merger occurring along the line of sight. This latter hypothesis would be consistent with the absence of a cool core in this cluster (Bauer et al. 2005).

A more detailed analysis of the connection between the radio halo and the cluster dynamics is in progress (Giacintucci et al., in prep.).

5.2. The core-halo in Z 7160

Z 7160 (z = 0.2578) is a compact Zwicky Cluster (ZwCl 1454.8+2223, NSCS J145715+222009), with little radio information available in the literature. On the 1.4 GHz NVSS image the cluster centre is dominated by a compact source, coincident with the central galaxy. At the higher resolution of the "Faint Images of the Radio Sky at 20 cm" (FIRST) survey (White et al. 1997) the radio source is pointlike. Chandra X-ray observations reveal that Z 7160 is a cooling core cluster (Bauer et al. 2005).

The 610 MHz image of the cluster is reported in Fig. 3, where a full resolution (left panel) and a tapered image (right panel) are shown. The central radio source consists of a compact component surrounded by an extended halo. The total flux density of the source only slightly increases going from the full resolution to the tapered image (from S = 38.0 ± 1.9 mJy to S = 43.6 ± 2.2 mJy), as well as the largest linear size, which goes from ∼50″ (∼ 200 kpc) to ∼90″ (∼360 kpc). Both flux density values include the compact component (associated with the dominant cluster galaxy) and the extended halo, whose origin is still debated (see for instance Mazzotta & Giacintucci 2008). The radio contours in the full resolution image show that the source has a sharp edge, and the larger extent of the low resolution image is the result of the convolution of positive residuals on the western side of the source with a larger restoring beam. In order to check if the extent of the central extended emission further increases at decreasing resolution, we imaged the cluster

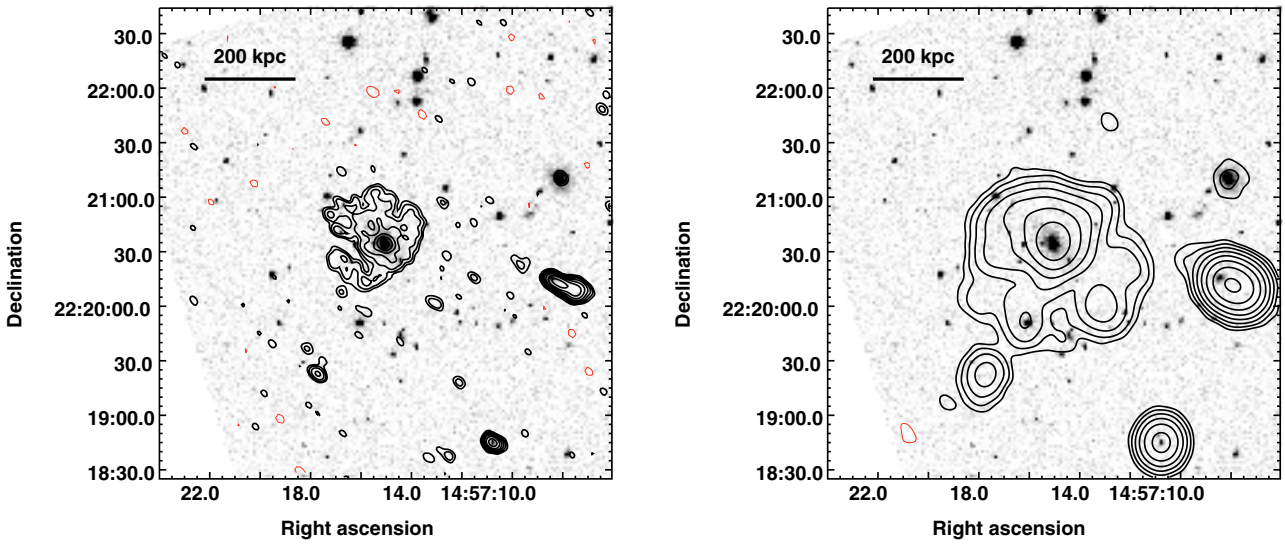

Fig. 3. *Left* – 610 MHz GMRT radio contours of Z 7160, overlaid on the optical red image from the SDSS. The resolution of the image is $5.9'' \times 4.6''$. The contour levels are $0.09 \times (\pm 1, 2, 4, 8, 16, 32, 64)$ mJy b^{-1}. The rms level (1σ) is 30 μJy b^{-1}. *Right* – Same portion of the optical sky with a 610 MHz $17'' \times 14''$ image overlaid. The radio contours are $0.12 \times (\pm 1, 2, 4, 8, 16, 32, 64, 128)$ mJy b^{-1}. The rms level (1σ) is 40 μJy b^{-1}. For this cluster $1'' = 3.965$ kpc.

at even lower resolutions, and obtained similar results in terms of integrated flux density and largest linear size. We therefore trust that the right panel of Fig. 3 detects all the 610 MHz radio emission.

The morphology, size and radio power of this source, $P_{610\ \mathrm{MHz}} = 8.25 \times 10^{24}$ W Hz^{-1}, coupled with its location in a cooling core, lead us to classify it as a core-halo source.

5.3. Peripheral diffuse radio emission in A 781

A 781 ($z = 0.2984$, richness class 2, Bautz-Morgan type III) has been studied very little at radio wavelengths. Its radio emission at 610 MHz is shown in Fig. 4, overlaid on the red plate of the DSS–2. The cluster field is characterised by a number of extended radio sources with optical counterparts, but the most outstanding feature is the extended low surface brightness emission peaking at $\mathrm{RA_{J2000}} = 09^{\mathrm{h}}20^{\mathrm{m}}32.2^{\mathrm{s}}$, $\mathrm{Dec_{J2000}} = 30°27'34.2''$. We will refer to this source as the "peripheral radio emission".

The insert in the left panel of Fig. 4 shows that this source has no obvious optical counterpart, either in the proximity of the peak or underlying the radio emission. Its flux density is $S_{610\ \mathrm{MHz}} = 32 \pm 2$ mJy, which corresponds to a radio power $P_{610\ \mathrm{MHz}} = 8.48 \times 10^{24}$ W Hz^{-1} if we assume that it is located at the cluster distance. At 1.4 GHz it is clearly visible on the NVSS, while it completely disappears in the FIRST survey (resolution of 5 arcsec). This is a further indication of its very low surface brightness. Using the NVSS flux density measurement we obtained a spectral index $\alpha^{1.4\ \mathrm{GHz}}_{610\ \mathrm{MHz}} = 0.76$. This value is not as steep as is usually found in diffuse cluster sources and dying radio galaxies, where observations report values $\alpha \gtrsim 1$ (e.g. Giovannini & Feretti 2004, and references therein for radio relics; and Parma et al. 2007, for dying radio galaxies).

The cluster was observed with Chandra (Obs. Id. 534, ACIS-I, exposure ~10 ks). The archival data were re-analysed by us in order to image the X-ray surface brigthness distribution, for comparison with the 610 MHz radio emission. Figure 5 shows the wavelet-reconstructed image in the 0.5–5.0 keV energy band, with 610 MHz radio contours overlaid.

The X-ray emission of the cluster is clearly complex. Beyond the emission coming from the cluster centre, a secondary peak is located in the western direction, and embeds a tailed radio galaxy. The peripheral radio emission is south–west of the main X-ray clump detected by Chandra, and is associated with the cluster centre. A third condensation of gas is visible south-east of the main X-ray emission. An optical analysis from a lensing survey reveals that the S-E X-ray condensation is coincident with another cluster at $z = 0.291$, i.e. the same distance of A 781 (Geller et al. 2005). The information available in the optical band is not sufficient to perform a detailed analysis of the dynamical state of the cluster.

The origin of the peripheral radio emission is unclear. The lack of an optical counterpart coupled with its location suggests that it might be a relic source; at the same time the value of the spectral index and its overall radio morphology suggests a tailed background radio source whose optical counterpart is too faint (or obscured) to be visible on the DSS-2. However, this last possibility seems implausible. No compact component is visible in the FIRST survey; moreover, the total radio power of this source, if located at the average cluster distance, is already at the upper end for typical tailed radio galaxies. A 327 MHz GMRT follow up of this source is in progress, to determine its origin.

5.4. A 1682 – A giant radio halo and two relics?

No high sensitivity and high resolution images are available in the literature for A 1682 ($z = 0.2260$, richness class 1, Bautz-Morgan type II). The strong central radio emission visible at 1.4 GHz on the NVSS image turns out to be the convolution of discrete sources after inspection of the cluster centre on the FIRST image.

Our GMRT 610 MHz images are reported in Fig. 6. The central radio emission in A 1682 is extremely complex. The double-peaked radio emission is coincident with a cluster galaxy ($z = 0.2180$) with a red magnitude (SDSS) $r = 16.50$ (see insert). Two tails depart from the inner region of the radio emission, however it is unclear if they are associated with the double radio galaxy. In the following we discriminate between "the

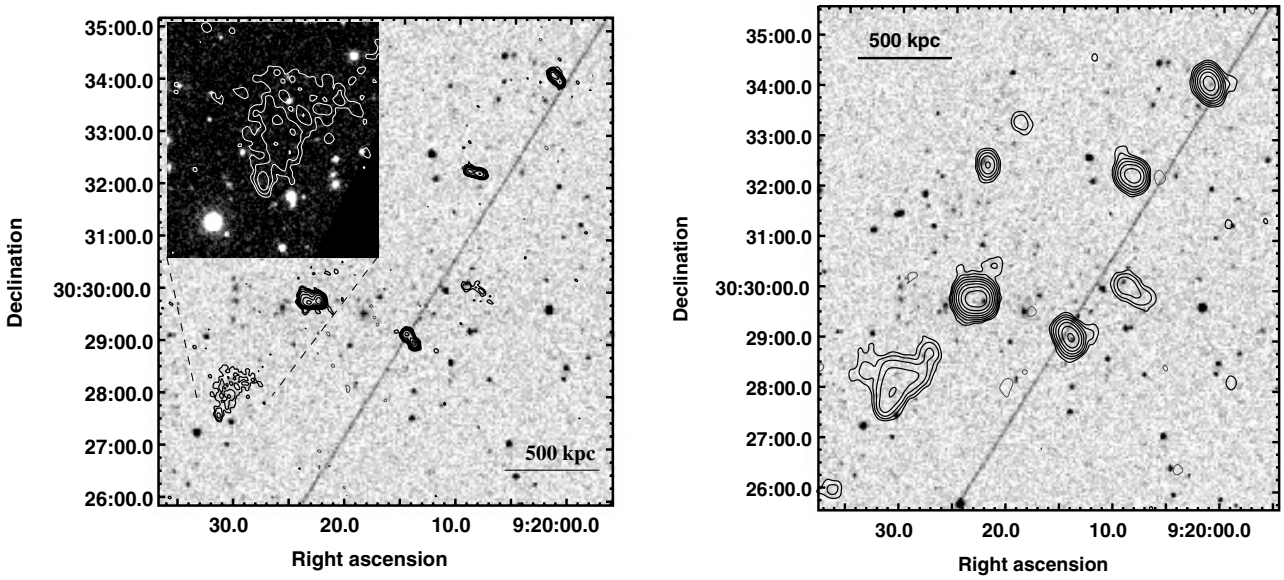

Fig. 4. *Left* – 610 MHz GMRT radio contours of A 781, overlaid on the DSS-2. The resolution of the image is 6″ × 5″. The contour levels are ±0.25, 0.5, 1, 2, 4, 8, 16 mJy b^{-1}. The rms level (1σ) is 50 μJy b^{-1}. The insert zooms onto the peripheral radio source, superposed on the SDSS red optical frame. *Right* – Same portion of the optical sky with a 610 MHz 18″ × 15″ image overlaid. The radio contours are ±0.3, 0.6, 1.2, 2.4, 4.8, 9.6, 19.2, 38.4 mJy b^{-1}. The rms level (1σ) is 50 μJy b^{-1}. For this cluster 1″ = 4.404 kpc.

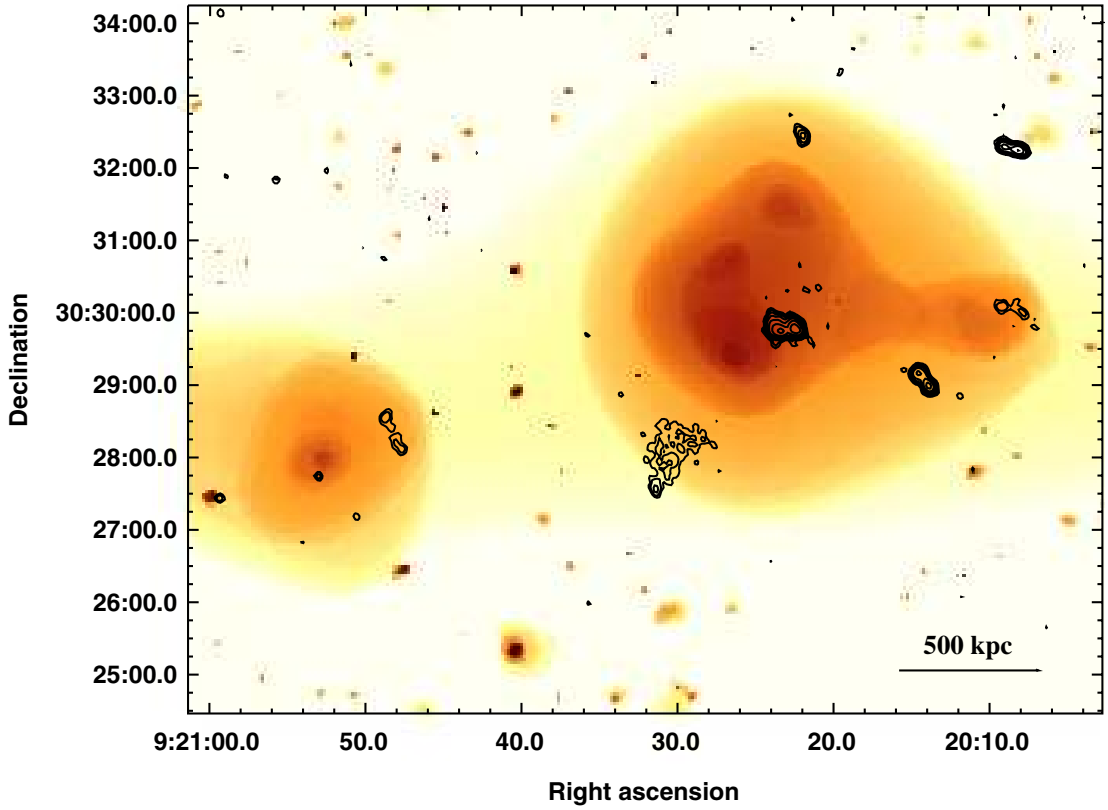

Fig. 5. 610 MHz GMRT radio contours of A 781, overlaid on the X-ray wavelet-reconstructed Chandra image in the 0.5–5.0 keV band. The resolution of the radio image is 6″ × 5″. The rms level (1σ) is 50 μJy b^{-1}. The contour levels are ±0.25, 0.5, 1, 2, 4, 8, 16 mJy b^{-1}.

eastern tail" and the "north-western ridge" (see labels in the figure). While the eastern tail is might be connected with the double-peakead source, the ridge (LAS ∼ 2′, LLS ∼430 kpc) is more puzzling. A possibility is that it is associated with another radio galaxy, however inspection of the radio-optical overlay shows that there is no obvious counterpart responsible for the radio emission (see Fig. 6 and insert). The lack of information at other radio frequencies does not allow any spectral analysis, which would be extremely useful to understand the nature of this ridge.

Two more outstanding radio features are noticeable in the images displayed in Fig. 6: (a) the ridge of emission located

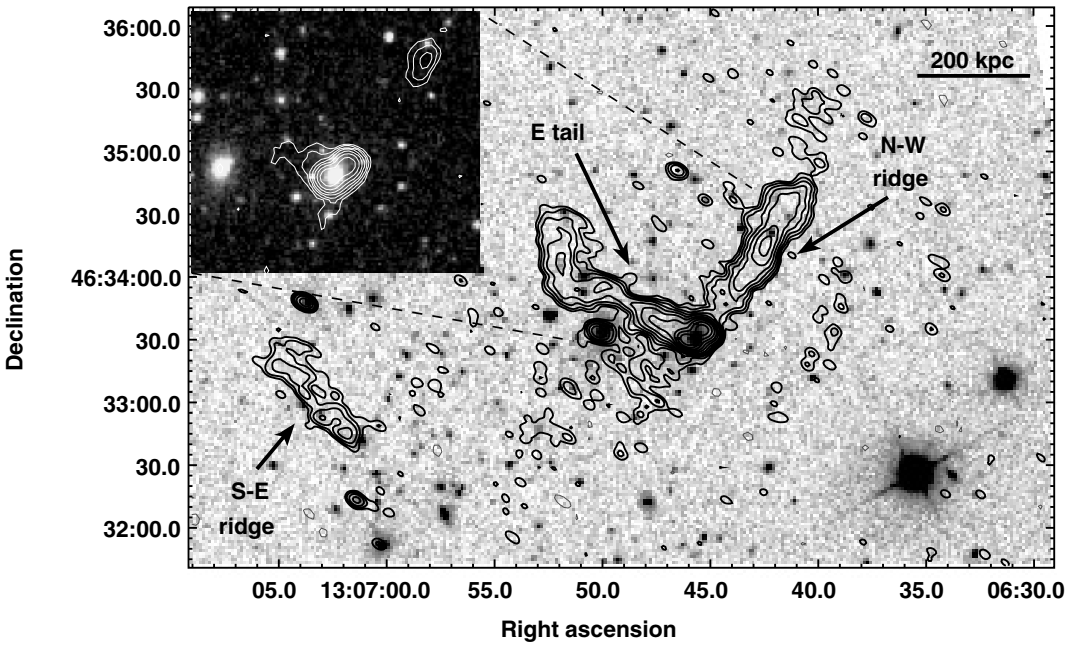

Fig. 6. 610 MHz GMRT radio contours of A 1682 on the optical red image from the SDSS. The resolution of the image is $6.2'' \times 4.1''$; the contour levels are $0.12\times$ (±)1, 2, 4, 8, 16, 32, 64, 128, 256, 512 mJy b^{-1}; the rms level (1σ) is 40 μJy b^{-1}. The insert shows the 1.4 GHz FIRST image of the cluster centre on the same optical frame. The resolution is $1.5''$. The radio contours are ±0.45, 0.9, 1.8, 3.6, 7.2, 14.4, 28.8, 57.6, 115.2 mJy b^{-1}. For this cluster $1'' = 3.593$ kpc.

south–east of the cluster centre (RA_{J2000} = 13^h05^m, Dec_{J2000} = 33°), labelled as the S–E ridge in the figure, and (b) positive residuals spread all around the cluster centre.

(a) The flux density of the S–E ridge is $S_{610\ MHz} = 15.5 \pm 0.8$ mJy, its LAS is ∼1′ (∼215 kpc). This structure is also visible on the NVSS, where we measured a flux density $S_{1.4\ GHz} = 6$ mJy. Due to the low resolution of the NVSS, this value also includes the contribution of the point source visible in Fig. 6 just north of the S–E ridge, whose flux density is $S_{610\ MHz} = 3.2 \pm 0.2$ mJy. We can give a rough estimate of the spectral index $\alpha^{1.4\ GHz}_{610\ MHz}$ of the S–E rigde assuming that the point source has a $\alpha^{1.4\ GHz}_{610\ MHz} = 0.7$, which is reasonable for a compact source. This value for α provides $S_{1.4\ GHz} = 1.8$ mJy, and hence the estimated spectral index for the ridge is $\alpha^{1.4\ GHz}_{610\ MHz} \sim 1.6$.

(b) The presence of positive residuals spread over a region of ∼4′ around the cluster centre was very clear during the imaging process, however the presence of the central radio galaxy did not allow a proper imaging of this emission. Due to the complexity of the central radio emission, an accurate subtraction of the discrete sources is not feasible. Nevertheless, we are confident that the positive residuals are significant. We estimated that the total flux density of the positive residuals, measured from the image shown in Fig. 7, is up to S_{res}(610 MHz) ∼ 44 mJy. This value was derived after subtracting the flux density of the discrete sources (the S-E and N-W ridges, the E-tail and the point sources) from the total flux density measured in a circular region with diameter of ∼4′. At the distance of A 1682 this corresponds to a linear scale of ∼860 kpc. Note that the flux density remains fairly constant even integrating over a larger portion of the sky around the cluster centre.

Figure 7 shows the 610 MHz radio emission of the cluster center overlaid on the Chandra X-ray emission. The X-ray image is the result of re-analysis of archive data (Obs. Id. 3244, ACIS-I, exposure ∼10 ks), carried out as for A 781. The gas distribution in A 1682 is clearly disturbed. It shows two condensations, the north-western being considerably brighter and more extended than the south-eastern one. The positive residuals in the radio image, referred to in (b), are all spread over the main X-ray condensation; the N–W ridge is located just outside the brightest X-ray part, while the S–E ridge occupies a region of faint X-ray emission.

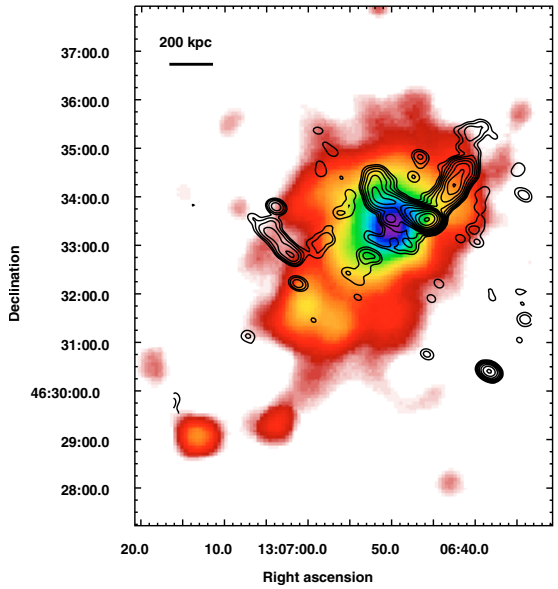

Fig. 7. 610 MHz GMRT radio contours of A 1682, overlaid on the X-ray smoothed Chandra image in the 0.5–5.0 keV band. The resolution of the radio image is $14.0'' \times 10.3''$. The rms level (1σ) is 50 μJy b^{-1}. The radio contours are $\pm 0.2 \times (1, 2, 4, 8, 16, 32, 64, 128, 256, 512, 1024)$ mJy b^{-1}.

The galaxy distribution of the cluster, derived from a weak lensing analysis (Dahle et al. 2002), confirms the perturbed

dynamical state: two peaks and a third minor condensation are found at the location of the main gas condensation.

According to the paradigm that cluster mergers provide energy to produce relativistic electrons, the perturbed dynamical state in A 1682 would be consistent with the hypothesis that it hosts a radio halo. The residual flux density we measured[2], $S_{\rm res}(610\ {\rm MHz}) \sim 44$ mJy, implies a radio power $P_{610\ {\rm MHz}} \sim 6.2 \times 10^{24}$ W Hz^{-1}. This value would be in agreement with the log $P_{1.4\ {\rm GHz}}$–log $L_{\rm X}$ correlation shown in a number of papers (e.g. Liang et al. 2000; CBS06) and scaled assuming $\alpha^{1.4\ {\rm GHz}}_{610\ {\rm MHz}} = 1.3$ (i.e. Brunetti et al. 2007). The overall appearance of the cluster, and the lack of an optical counterpart for the S–E and N–W ridges, suggest that these regions of radio emission might be connected with merging processes, and one possibility is that they are relic sources. Low frequency radio follow up for this cluster is in progress and a more detailed analysis will be presented in a forthcoming paper.

5.5. Candidate extended emission at the centre of Z 2661

Z 2661 is a compact Zwicky Cluster (Zw 0947.2+1723), the most X-ray luminous and the second most distant in the sample, at $z = 0.3825$ (see Table 1). Very little radio and X-ray information exists in the literature. Chandra X-ray observations are available from the archive, and 1.4 GHz images are available from the NVSS and FIRST surveys. An elongated diffuse source is visible on the NVSS in the central part of the cluster, with a largest linear size ∼3′. Inspection of the FIRST image shows that only a faint point-like source is located within the extended emission on the NVSS.

The radio emission of Z 2661 at 610 MHz is shown in Fig. 8, where a full resolution (left panel) and tapered image (right panel) are shown overlaid on the DSS-2. The most relevant feature in the $17'' \times 17''$ resolution image (right panel) is the extended emission visible around the three discrete radio sources in the central cluster region, partially coincident with the diffuse emission visible on the NVSS, as shown in Fig. 9. In order to highlight this emission, we subtracted from the *u-v* data all the discrete sources visible in the full resolution image of the whole cluster field, and produced an image of the residuals using only the shortest baselines and natural weighting. The resulting image is shown in Fig. 10, superposed on the Chandra X-ray image, which was obtained from a re-analysis of data available from the public archive (Obs. Id. 3274, ACIS–I, exposure ∼15 ks).

The X-ray morphology of Z 2661 looks only marginally perturbed, however a change in position angle of the isodensity colours with changing distance from the cluster centre suggests that projection effects might play a role in the overall appearance of the brightness distribution. The radio-X overlay clearly shows that the extended residual emission is located on the peak of the X-ray surface brightness of the intracluster gas. The spatial coincidence between the thermal and non-thermal emission is a further hint that the residuals might belong to a diffuse cluster radio source.

The total flux density of this emission ranges from ∼4 to ∼5.9 mJy, depending on the size of the region considered for the integration. Based on our analysis on the upper limits described in Sect. 4, such residual values are expected in the case of radio halos with total injected flux density $S_{\rm inj} \approx 10 \div 15$ mJy. We thus consider this case a "suspect" diffuse emission. Using the measured flux density, the radio power of the extended emission at the centre of Z 2661 would be in the range $P_{610\ {\rm MHz}} \sim 2$–$3 \times 10^{24}$ W Hz^{-1}; the angular size of the imaged emission is ∼1′ (∼310 kpc). We stress however that these values are very uncertain and refer only to the information provided by the images. Radio observations at lower frequency are necessary to confirm and further study this emission.

5.6. Notes on the clusters with VLA archive data

A number of clusters belonging to the sample in Table 1 were not observed as part of the GMRT radio halo survey either because they belong to other GMRT programs (i.e. the GMRT cluster key project), or because of the existence of VLA archival data.

We retrieved and re-analysed 1.4 GHz VLA D– configuration archival data of A 1763 (Obs. Id. AC696), A 2111 (Obs. Id. AG639), A 2261 (Obs. Id. AC696). No hint of large scale emission was found in A 1763 and A 2111. The case of A 2261 is more uncertain, due to the presence of strong and extended sources at the cluster centre. In the attempt to further investigate the nature of the central emission in this cluster, we also re-analysed 1.4 GHz VLA B-configuration archival data (Obs. Id. AC696) and combined the two arrays. The resulting images are shown in Fig. 11, where the radio contours of the D (red) and B+D (black) arrays are reported, overlaid on the DSS-2. Even though a detailed analysis is not possible, due to some problems with the flux density scale of the two arrays, our images show that some extended emission might be present around the dominant galaxy over an angular scale of $4' - 5'$ (∼850–1000 kpc). An accurate subtraction of the contribution from the discrete sources (unfeasible with the available archival data) is needed to clarify the situation.

6. Discussion of the GMRT radio halo survey observational results

We summarize the most important results reported in this work, and give a brief discussion of the results of the whole sample, including the literature information and those presented in Paper I. No information is available in the literature for the five clusters marked with √ in Table 1. An overview of the diffuse cluster sources found in the GMRT radio halo survey is reported in Table 4.

6.1. Cluster centres

6.1.1. Radio halos and candidates

Among the clusters presented in this paper, a new giant (LLS ∼890 kpc) radio halo was discovered in A 697. This brings to 10 the total number of clusters with a radio halo in our selected sample. In particular: A 2744, A 1300, A 2163, A 773, A 1758a and A 2219 have literature information (see Table 1); A 209, A 697, RXCJ 1314.4–2515 and RXCJ 2003–2323 were found with the GMRT radio halo survey. They are all giant halos, except RXCJ1314.4–2515 (see Table 4).

A candidate giant radio halo was found in A 1682 (Sect. 5.4). We found residual emission of ∼44 mJy, spread over a linear scale of the order of ∼860 kpc. The very unrelaxed morphology of the cluster would argue in favour of the presence of a giant radio halo, which we were unable to properly image with the 610 MHz data due to the highly complex radio emission at the

[2] We note that the complex radio emission at the centre of A 1682 makes this cluster very different from those selected for the analysis on the upper limits. For this reason no direct comparison can be made between this cluster and the flux density upper limits to the radio halo detection estimated in Sect. 4.

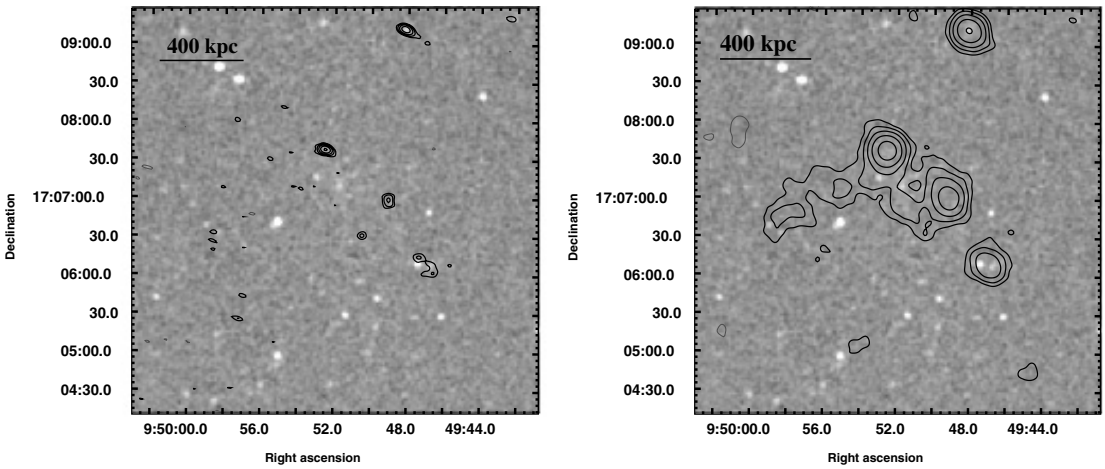

Fig. 8. *Left* – 610 MHz GMRT radio contours of Z 2661, overlaid on the DSS-2. The resolution of the image is 6.5″ × 4.5″, PA 80°. The contour levels are ±0.25, 0.5, 1, 2, 4, 8, 16 mJy b^{-1}. The rms level (1σ) is 65 μJy b^{-1}. *Right* – Same portion of the radio sky with a 610 MHz 17.7″ × 17.4″ image overlaid. The radio contours are ±0.25, 0.5, 1, 2, 4, 8 mJy b^{-1}. The rms level (1σ) is 65 μJy b^{-1}. For this cluster 1″ = 5.196 kpc.

Table 4. Results of the GMRT Radio Halo Survey. Halos, relics and candidates.

Cluster	Source Type	$S_{610\ \mathrm{MHz}}$ mJy	log $P_{610\ \mathrm{MHz}}$ W Hz^{-1}	LAS arcmin	LLS kpc	Axial Ratio
A 209*	Giant Halo	24.0 ± 3.6	24.46	~4	~810	~2
RXCJ 2003.5–2323*	Giant Halo	96.9 ± 5.0	25.49	~5	~1400	~1.3
A 697	Giant Halo	13.0 ± 2.0	24.54	~3.5	~890	~1
RXCJ 1314.4–2515*	Western Relic	64.8 ± 3.2	25.03	~4	~910	~3
	Eastern Relic	28.0 ± 1.4	24.67	~4	~910	~4.3
	Halo	10.3 ± 0.3	24.22	~2	~460	~1.5
A 521*	Relic	41.9 ± 2.1	24.91	~4	~930	~4.5
A 3444*	Central Galaxy	16.5 ± 0.8	24.51	~0.7	~165	~1.4
	surrounding Halo	10.0 ± 0.8	24.29	~1.5	~350	~1.4
Z 7160	Core-halo	43.6 ± 2.2	24.92	~1.5	~360	~1
A 781	Candidate relic?	32.0 ± 2.0	24.92	~2	~520	~1.7
A 1682$^\diamond$	Candidate halo?	~44	24.79	~4	–	–
Z 2661$^\clubsuit$	Candidate halo?	~5.9	24.47	–	–	–

* Information from Paper I. $^\diamond$ See Sect. 5.4. $^\clubsuit$ See Sect. 5.5.

cluster centre. Follow up observations are in progress to confirm this result.

"Suspect" extended emission was found at the centre of Z 2661 (Sect. 5.5), the second most distant and second most X-ray luminous cluster in the sample. It is possible that we are imaging only the peak brightness of a brighter and larger structure. Follow up observations at lower frequencies are necessary to confirm this result.

The re-analysis of archival VLA data shows that the central region of A 2261 (Sect. 5.6) is complex and puzzling, due to the presence of many individual sources and to the very extended emission associated with a cluster FRI galaxy (Fanaroff & Riley 1974). Further investigation is necessary to disentangle the contribution of the individual sources from possible extended emission on the cluster scale.

Finally, three clusters in the sample host central extendend radio emission, though of different origin. The nature of the central radio emission in A 2390 (Bacchi et al. 2003) is still debated and it is unclear if it is a mini-halo source (see Gitti et al. 2004, for details on this class of extended radio sources) or a radio halo of small size; a core-halo source was found in the cool core cluster Z 7160 (Sect. 5.2), and candidate extended emission, possibly associated with the dominant cluster galaxy, was found in A 3444 (Paper I).

6.1.2. Non detections and upper limits

Our work confirms that radio halos are a rare phenomenon. One of the main results presented here and in Paper I is that most of the clusters in our sample do not show central extended emission.

Among the 34 clusters observed with the GMRT radio halo survey, 25 lack a central extended source at the sensitivity level of the observations. For 20 of them we derived firm upper limits to the radio power of a giant radio halo by means of a radio analysis carried out on typical GMRT *u-v* data sets and using the rms noise in the final images (Sect. 4). For the remaining five clusters we did not derive the upper limits, since the rms noise in the final images is considerably higher than the average quality of our survey (see Table 2). Such clusters will not be considered in Sect. 6.4.

Furthermore, no emission was found with the VLA in RXCJ 0437.1+0043 (Feretti et al. 2005), in A 1763 and A 2111, whose archival data were re-analysed here (Sect. 5.6).

6.2. Cluster outskirts. Radio relics and candidates

The 610 MHz GMRT radio halo survey turned out also to be successful for the study of the peripheral cluster regions, where relic

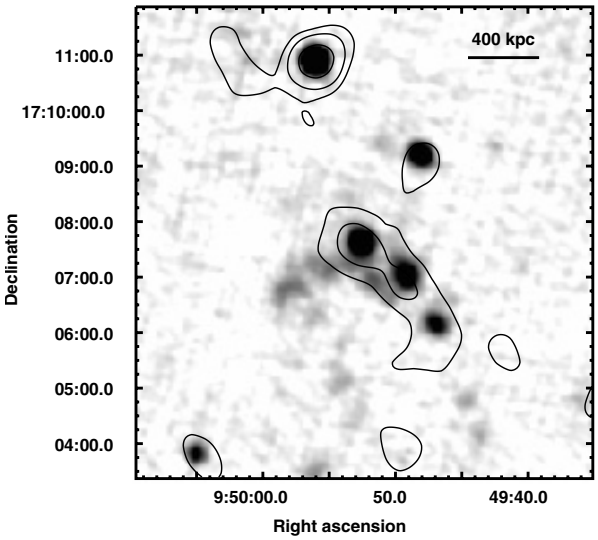

Fig. 9. Grey scale GMRT 610 MHz emission of Z 2661 (same image as in the right panel of Fig. 8), with 1.4 GHz NVSS contours overlaid. The contour levels are ±1, 2, 4 mJy b^{-1}.

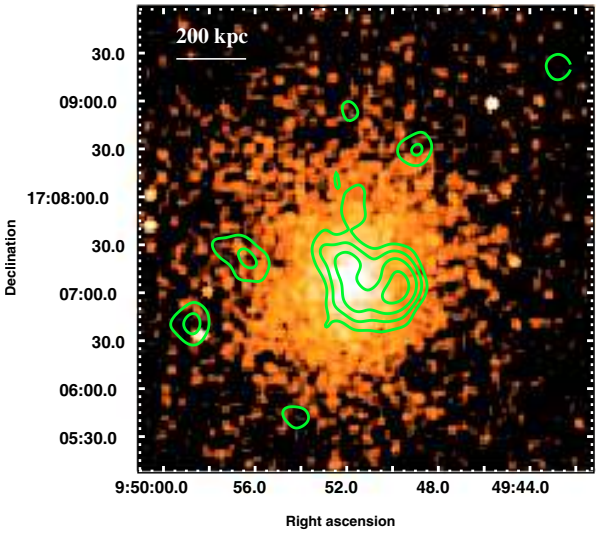

Fig. 10. 610 MHz GMRT contours of the central residual emission in Z 2661, overlaid on the smoothed Chandra image in the 0.5–5.0 keV energy band. The restoring beam is 20″ × 20″. Contours are ± 0.15, 0.3, 0.5, 0.8 mJy b^{-1}. The average rms close to the central residuals is ∼40 μJy b^{-1}.

sources are usually found. Our knowledge of the origin of radio relics is still limited. At this stage, a clear correlation exists between the presence of relics and dynamical activity in the hosting clusters, and all models proposed so far to explain the origin of relics invoke the presence of a merger shock (e.g. Enßlin et al. 1998; Roettiger et al. 1999; Enßlin & Gopal-Krishna 2001; Markevitch et al. 2005). However, only a few relics have been studied in detail so far, and new detections of relic sources are crucial to improve our understanding of the origin of these sources.

We found a relic in A 521 (Paper I; Giacintucci et al. 2006, 2008) and a double relic in RXCJ 1314.4–2515 (Paper I; Feretti et al. 2005). RXCJ 1314.4–2515 is a unique case of a cluster with a double relic and a radio halo. We are studying both clusters over a wide range of radio frequencies.

Two more clusters deserve further investigation. Peripheral extended emission, whose origin is unclear, was detected in

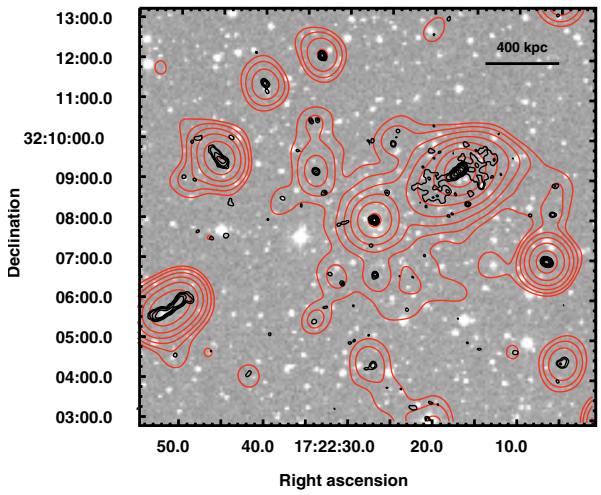

Fig. 11. 1.4 GHz emission in A 2261 overlaid on the DSS-2 optical image. Red contours: D-array, resolution of 44.6″ × 41.3″, contour levels ±0.15, 0.3, 0.6 ... mJy b^{-1}, 1σ rms 50 μJ b^{-1}. Black contours: B+D array, resolution 6.3″ × 5.7″, contour levels ±0.09, 0.18, 0.36 ... mJy b^{-1}, 1σ rms 30 μJ b^{-1}. For this cluster 1″ = 3.568 kpc.

A 781 (Sect. 5.3); two intriguing "ridges" of radio emission were found in A 1682, elongated in shape and with no optical counterpart (Sect. 5.4). The X-ray information on both clusters suggests complex dynamics.

6.3. Information on the cluster dynamics from X-ray data

It is fairly well established that all clusters hosting halos and relics show signs of merging activity (e.g. Buote 2001; Schuecker et al. 2001), while a complete analysis of the dynamics of clusters without halos and relics is still missing. A huge amount of data would be necessary to perform such study in the optical band, and our main source of knowledge is the information of the gas distribution available from the X-ray data archives.

In order to collect some information on the dynamical state for each cluster in our sample, based either on the mass and/or intracluster gas distribution, we searched the literature (Dahle et al. 2002; Zhang et al. 2006). Furthermore we consulted the X-ray public archives (ROSAT, Chandra, ASCA and XMM) and carried out a zero-order data reduction for imaging purposes (i.e. no data analysis) for all clusters (regardless of their radio properties) without literature information and with public observations in the Chandra and/or XMM archive.

Our investigation reinforces our earlier findings and the literature information: all clusters hosting halos and/or relics and those with candidate extended emission show signatures of dynamical activity, i.e. asymmetries and substructure in the X-ray emission, elongation and/or multiple peaks in the distribution of the mass (see Paper I, references in Table 1 and Sects. 5.1, 5.3, 5.4 and 5.5).

24 clusters in our complete sample do not host diffuse extended emission of any kind. This number includes 19 upper limits in Table 3 (we dropped RXCJ 2228.6+2037 due to the redshift), A 1763 and A 2111 (Sect. 5.6), RXCJ 0437.1+0043 (Feretti et al. 2005), and the two clusters A 3444 (Paper I) and Z 7160 (Sect. 5.2), whose central emission seems connected to the central galaxy. No information was found for three clusters (Z 5768, RXCJ 1512.2–2254 and Z 5699). From a visual

inspection of the X-ray images for the remaining 21 we found that:

(a) seven clusters show a fairly regular gas distribution, and they do not seem to be undergoing dynamical activity;
(b) 14 clusters show irregular distribution of the intracluster gas, in the form of elongation, multiple clumps, change of boxiness at different cluster radii. These morphologies are suggestive of some form of dynamical activity;
(c) if we divide our clusters into two bins of X-ray luminosity and define a "high" luminosity and a "low" luminosity interval, with the separation at $L_X \approx 8 \times 10^{44}$ erg s^{-1} (see also Cassano et al. 2008), regular and disturbed clusters are equally found in both intervals.

Our qualitative findings are corroborated by a comparison of the results for our sample and the work of Hart (Ph.D. Thesis, private communication), who studied the X-ray morphology for a sample of 143 galaxy clusters with available Chandra public observations by means of a multiple–moment power ratio analysis (Buote & Tsai 1995).

A number of clusters in our sample are included in the X-ray analysis by Hart and for them we could cross-correlate the radio properties (presence of cluster diffuse emission or lack thereof) with a quantitative indicator of the distribution of the X-ray intracluster gas. The results are reported in Fig. 12, which shows the location of the clusters in the P_2/P_0–P_3/P_0 plane. Each P_n represents the square of the nth multipole of the two–dimensional pseudopotential generated by the X-ray surface brightness evaluated over a circular aperture. The ratio P_2/P_0 is a measurement of the ellipticity, and P_3/P_0 is related to the presence of multiple peaks in the X-ray distribution (see Buote 2001 for details of these parameters). Low values both of P_2/P_0 and of P_3/P_0 indicate little deviation from spherical symmetry and may be considered indicators of relaxation; the dotted line is a tentative separation between small and large deviations from symmetry.

Some interesting conclusions can be drawn from the figure. The clusters below the dotted line may be considered relaxed clusters, and none of them hosts diffuse cluster emission of any kind; those above the line, which show large deviations from symmetry and may be considered perturbed clusters, include radio halos, relics, candidates for both classes, as well as clusters without diffuse radio sources.

6.4. Fraction of clusters hosting a radio halo

A preliminary estimate of $f_{\rm RH}$, the fraction of clusters in our sample that host a radio halo, can finally be given. Unfortunately the radio information is not complete for all clusters in the sample, so in the normalization we cannot include the 5 clusters marked with $\surd$ in Table 1. We further exclude the 5 clusters with high rms (see Sect. 4), those with suspected central diffuse emission (A 521, A 2261, Z 2661 and A 1682, see Sects. 4 and 6.1.1), and the cluster RXCJ 2228.6+2037, whose redshift is just above the limit of our selection criteria (see Table 1). Therefore the fraction is $f_{\rm RH} 10/35 = 29 \pm 9\%$.

Most of the clusters with a radio halo, i.e. 9/10, are found in the high X-ray luminosity bin, where the fraction of clusters with a radio halo is as high as $f_{\rm RH} 9/24 = 38 \pm 13\%$. We point out that the uncertainty in $f_{\rm RH}$ is derived on the basis of the detections only.

Giovannini et al. (1999) cross-correlated the X-ray Brightest Abell clusters (XBACs sample) with the NVSS for the local Universe ($z \leq 0.2$) and found that the occurrence of cluster halos and relics is higher in clusters with high X-ray luminosity and high temperature. Our result confirms those findings, i.e. at higher redshift clusters with high X-ray luminosity have a higher probability of hosting a radio halo. A detailed analysis of the statistics on the occurrence of radio halos over the redshift range 0.05–0.4 was carried out in Cassano et al. (2008).

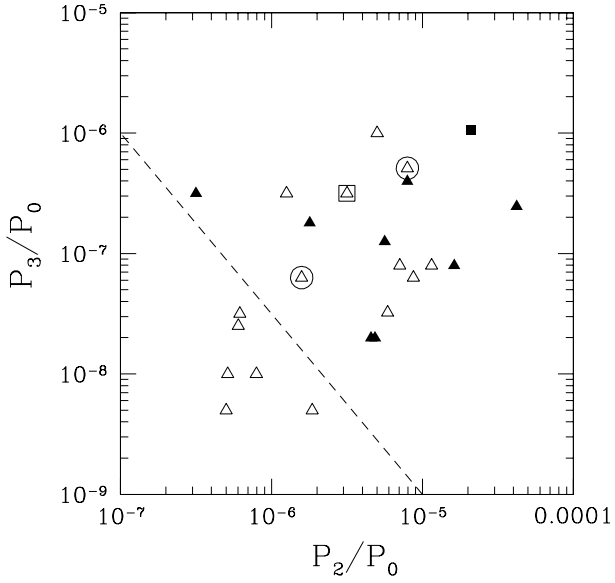

Fig. 12. Location of clusters with and without extended cluster scale emission on a $P_2/P_0 - P_3/P_0$ plot. Filled triangles: clusters with radio halo; empty triangles: clusters without radio halo; filled square: cluster with radio relic; empty triangles inside a circle: clusters with candidate halo; empty triangle inside a square: clusters with candidate relic. The dotted line divides the relaxed and perturbed clusters.

7. Summary and conclusions

The GMRT radio halo survey, carried out at 610 MHz, was designed to investigate the link between the presence of diffuse cluster scale emission and the dynamics of the hosting clusters in the redshift interval 0.2–0.4, where in the framework of the re–acceleration model the bulk of radio halos is expected. We selected a complete sample of massive clusters with $L_X(0.1\text{–}2.4\ \text{keV}) > 5 \times 10^{44}$ erg s^{-1}, and $0.2 < z \leq 0.4$ from the ROSAT-ESO Flux Limited X-ray galaxy cluster catalogue and from the extended ROSAT Brightest Cluster Sample. Declination limits were also imposed (Sect. 2).

34 clusters in the sample lacked high sensitivity information in the literature and in the radio archives, and were observed with the GMRT at 610 MHz. Imaging was carried out over a wide range of resolutions, with a sensitivity in the average range 35–100 μJy b^{-1}. We also retrieved and analyzed unpublished archive VLA observations for three clusters in the sample. 11 GMRT clusters were presented in Paper I, the remaining are presented in this paper. The main results of the GMRT radio halo survey can be summarized as follows.

(1) Diffuse emission on the cluster scale was found in a number of clusters. In particular, we detected: 4 radio halos, bringing to 10 their number in the whole sample; three relic sources; one core-halo cluster. Moreover, we found a candidate giant radio halo, suspect emission at the centre of one cluster, a candidate relic and a candidate core-halo source. For all clusters with candidate extended emission, follow-up observations are in progress.
(2) Most of the clusters observed with the GMRT do not show diffuse central emission, and this result confirms that radio

halos are not common. Thanks to the high quality of our data we managed to place firm radio power upper limits in 20 clusters.

(3) For those clusters with available X-ray information, we carried out an X-ray/radio analysis. Our results confirm that all clusters hosting halos, relics and candidate diffuse emission show signature of dynamical activity. Furthermore, we find that clusters without diffuse emission may be both relaxed and perturbed. Finally, none of the relaxed clusters hosts diffuse emission. A more quantitative analysis would be required in order to assess the amount of turbulent energy that might be available in the framework of the re-acceleration model.

(d) The fraction of clusters in our sample with a central radio halo is $f_{\rm RH} = 29 \pm 9\%$. This fraction seems to show some dependence on the X-ray luminosity of the hosting cluster. If we define a "low" and a "high" X-ray luminosity bin, with a threshold chosen at $L_{\rm X} \approx 8 \times 10^{44}$ erg s^{-1} (for consistency with Cassano et al. 2008) we find that the fraction of clusters with a radio halo in the high X-ray luminosity range is as high as $f_{\rm RH} = 38 \pm 13\%$. This result extends to intermediate redshift the findings of Giovannini et al. (1999) for the local Universe ($z \leq 0.2$).

The results of the GMRT radio halo survey have provided observational support to the re-acceleration scenario for the formation of radio halos. In such a scenario, particles are re-accelerated by magneto-hydrodynamic turbulence injected in the ICM during cluster-cluster mergers. A basic expectation of this model is that only massive clusters undergoing sufficiently energetic merger events can host a giant radio halo. In addition, the finite dissipation time-scale of turbulence implies that radio halos should be "transient" phenomena, with a duration of the order of $\sim$1 Gyr or less. This is a major difference between the primary and secondary electron model scenario, the latter predicting that radio halos should be very common in galaxy clusters, should be long lived phenomena and are not expected to show any correlation with the cluster dynamical status.

In this respect the newest and most relevant result of our survey concerns the non-detections and the well constrained upper limits for a large fraction of the sample objects, at a level which is below at least one order of magnitude of the radio power expected on the basis of the well known $P_{1.4\ \rm GHz}$–$L_{\rm X}$ correlation for giant radio halos in the same X-ray luminosity interval. This gap indicates a bimodal behaviour in the radio emission properties of massive clusters and strongly supports the re-acceleration model whereby the giant radio halos are temporary, although impressive, events related to the recent occurrence of large mergers, as we have recently discussed (BVD07).

As a final point we would like to stress the importance of our GMRT survey, which provides new statistical basis on the occurrence of giant radio halos in the critical redshift range 0.2–0.4. The combination of our results with those of the lower redshift samples shows that there is good statistical evidence (at 3.6σ) for an increase in the occurrence of giant radio halos with increasing X-ray luminosity (mass), in agreement with the prediction of the reacceleration model, as extensively discussed in Cassano et al. (2008).

Acknowledgements. We thank the staff of the GMRT for their help during the observations. GMRT is run by the National Centre for Radio Tata Institute of Fundamental Research. We acknowledge the financial contribution from the Italian Ministry of Foreign Affairs, from grants MIUR PRIN2004, PRIN2005 and 2006, from PRIN–INAF2005, and from contract ASI–INAF I/023/05/0.

References

Bacchi, M., Feretti, L., Giovannini, G., et al. 2003, A&A, 400, 465
Bauer, F. E., Fabian, A. C., Sanders, J. S., et al. 2005, MNRAS, 359, 1481
Blasi, P., & Colafrancesco, S. 1999, APh, 12, 169
Blasi, P. 2004, JKAS, 37, 483
Böhringer, H., Schuecker, P., Guzzo, L., et al. 2004, A&A, 425, 367
Brunetti, G. 2003, in Matter and Energy in Clusters of Galaxies, ed. S. Bowyer, & C.-Y. Hwang (San Francisco: Astron. Soc. Pac.), ASP Conf. Ser., 301, 349
Brunetti, G. 2004, JKAS, 37, 493
Brunetti, G., Setti, G., Feretti, L., et al. 2001, MNRAS, 320, 365
Brunetti, G., Venturi, T., Dallacasa, D., et al. 2007, ApJ, 670, L5
Buote, D. A. 2001, ApJ, 553, 15
Buote, D. A., & Tsai, J. C. 1995, ApJ, 452, 522
Cassano, R., & Brunetti, G. 2005, MNRAS, 357, 1313 (CB05)
Cassano, R., Brunetti, G., & Setti, G. 2004, JKAS, 37, 589
Cassano, R., Brunetti, G., & Setti G. 2006, MNRAS, 369, 1577 (CBS06)
Cassano, R., Brunetti, G., Venturi, T., et al. 2008, A&A, 480, 687
Condon, J. J., Cotton, W. D., Greisen, E. W., et al. 1998, AJ, 115, 1693
Dahle, H., Kaiser, N., Irgens, R. J., et al. 2002, ApJS, 139, 313
Dennison, B. 1980, ApJ, 239, 93
Dolag, K., & Enßlin, T. A. 2000, A&A, 362, 151
Ebeling, H., Edge, A. C., Böhringer, H., et al. 1998, MNRAS, 301, 881
Ebeling, H., Edge, A. C., Allen, S. W., et al. 2000, MNRAS, 318, 333
Enßlin, T. A., & Gopal–Krishna 2001, A&A, 366, 26
Enßlin, T. A., Biermann, P. L., Klein, U., et al. 1998, A&A, 332, 395
Fanaroff, B. L., & Riley, J. M. 1974, MNRAS, 167, 31
Feretti, L., 2005, in X-ray and radio connections, ed. L. O. Sjouwerman, & K. K. Dyer, published electronically by NRAO, http://www.aoc.nrao.edu/events/xraydio
Feretti, L., Fusco-Femiano, R., Giovannini, G., et al. 2001, A&A, 373, 106
Feretti, L., Schuecker, P., Böhringer, H., et al. 2005, A&A, 444, 157
Ferrari, C., Govoni, F., Schindler, S., et al. 2008, Space Sci. Rev., 134, 93
Fusco-Femiano, R., Orlandini, M., Brunetti, G., et al. 2004, ApJ., 602, L73
Fusco-Femiano, R., & Orlandini, M. 2008, [arXiv:0802.1817]
Geller, M. J., Dell'Antonio, I. P., Kurtz, M. J., et al. 2005, ApJ, 635, L125
Giacintucci, S. 2007, Ph.D. Thesis, University of Bologna
Giacintucci, S., Venturi, T., Bardelli, S., et al. 2006, New Astron., 11, 437
Giacintucci, S., Venturi, T., Macario, G., et al. 2008, A&A, in press [arXiv:0803.4127]
Giovannini, G., & Feretti, L. 2004, J. Korean Astr. Soc., 37(5), 323
Giovannini, G., Tordi, M., & Feretti, L. 1999, New Astron., 4, 141
Giovannini, G., Feretti, L., Govoni, F., et al. 2006, AN, 327, 563
Girardi, M., Boschin, W., & Barrena, R. 2006, A&A, 455, 45
Gitti, M., Brunetti, G., Feretti, L., et al. 2004, 417, 1
Govoni, F., & Feretti, L. 2004, Int. J. Mod. Phys. D, 13, 1549
Govoni, F., Feretti, L., Giovannini, G., et al. 2001, A&A 376, 803
Herbig, T., & Birkinshaw, M. 1994, BAAS, 26, 1403
Kempner, J. C., & Sarazin, C. L. 2001, ApJ, 548, 639
Liang, H., Hunstead, R. W., Birkinshaw, M., et al. 2000, ApJ, 544, 686
Markevitch, M., Govoni, F., Brunetti, G., et al. 2005, ApJ, 627, 733
Mazzotta, P., & Giacintucci, S. 2008, ApJ, 675, L9
Parma, P., Murgia, M., de Ruiter, H.-R., et al. 2007, A&A, 470, 875
Petrosian, V. 2001, ApJ, 557, 560
Petrosian, V., & Bykov, A. 2008, Space Sci. Rev., 134, 207
Pfrommer, C., Springel, V., Enßlin, T. A., et al. 2006, MNRAS, 367, 113
Rephaeli, Y., Nevalainen, J., Ohashi, T., et al. 2008, Space Sci. Rev., 134, 191
Reid, A. D., Hunstead, R. W., Lemonon, L., et al. 1999, MNRAS, 302, 571
Rengelink, R. B., Tang, Y., de Bryun, A. G., et al. 1997, A&AS, 124, 259
Ryu, D., Kang, H., Hallman, E., et al. 2003, ApJ, 593, 599
Roettiger, K., Burns, J. O., & Stone, J. M. 1999, ApJ, 518, 603
Rossetti, M., & Molendi, S. 2004, A&A, 414, L41
Sarazin, C. L. 1999, ApJ, 520, 529
Sarazin, C. L. 2004, JKAS, 37, 433
Schuecker, P., Böhringer, H., Reiprich, T. H., et al. 2001, A&A, 378, 408
Venturi, T., Giacintucci, S., Brunetti, G., et al. 2007, A&A, 463, 937 (Paper I)
White, R. L., Becker, R. H., Helfand, D. G., et al. 1997, ApJ, 475, 479
Zhang, Y.-Y., Böhringer, H., Finoguenov, A., et al. 2006, A&A, 456, 55